The role of creep in the time-dependent resistance of Ohmic gold contacts in radio frequency microelectromechanical system devices

O. Rezvanian,[1] C. Brown,[2] M. A. Zikry,[1] A. I. Kingon,[3] J. Krim,[2] D. L. Irving,[3] and D. W. Brenner[3,a)]

[1]*Department of Mechanical and Aerospace Engineering, North Carolina State University, Raleigh, North Carolina 27695, USA*
[2]*Department of Physics, North Carolina State University, Raleigh, North Carolina 27695, USA*
[3]*Department of Materials Science and Engineering, North Carolina State University, Raleigh, North Carolina 27695, USA*

(Received 29 December 2007; accepted 2 May 2008; published online 28 July 2008)

It is shown that measured and calculated time-dependent electrical resistances of closed gold Ohmic switches in radio frequency microelectromechanical system (rf-MEMS) devices are well described by a power law that can be derived from a single asperity creep model. The analysis reveals that the exponent and prefactor in the power law arise, respectively, from the coefficient relating creep rate to applied stress and the initial surface roughness. The analysis also shows that resistance plateaus are not, in fact, limiting resistances but rather result from the small coefficient in the power law. The model predicts that it will take a longer time for the contact resistance to attain a power law relation with each successive closing of the switch due to asperity blunting. Analysis of the first few seconds of the measured resistance for three successive openings and closings of one of the MEMS devices supports this prediction. This work thus provides guidance toward the rational design of Ohmic contacts with enhanced reliabilities by better defining variables that can be controlled through material selection, interface processing, and switch operation. © *2008 American Institute of Physics*. [DOI: 10.1063/1.2953072]

I. INTRODUCTION

Radio frequency microelectromechanical system (rf-MEMS) devices use two types of switches; capacitive switches, which have dielectric contacts, and Ohmic switches, which have conducting contacts.[1] For most applications, capacitive switches traditionally have longer lifetimes and better reliabilities than Ohmic switches. This is due in part because the adhesion of capacitive contacts can be made relatively weak, while the requirement of small contact resistances for Ohmic switches require metal-metal contacts that can be susceptible to cold welding and strong adhesion. To effectively engineer Ohmic switches with optimized performance, a better understanding of the mechanics of metal contacts is needed, as well as how the associated processes are related to contact resistance.

In a recent study, Rezvanian *et al.* compared the time-dependent contact resistance between two loaded rough gold surfaces calculated by a specialized finite-element plasticity model to experimental measurements of the time-dependent resistance of a rf-MEMS device containing a closed gold Ohmic switch.[2] The calculated and experimental measurements had very similar trends. Both showed a relatively large initial drop in resistance over a time period of up to a few minutes, followed by an apparent plateau in the resistance. For the experiment, the initial closure of the switch resulted in a plateau value of about 2 Ω, while opening and then closing the switch two times resulted in plateau values of about 2.8 and 4 Ω, respectively. The plateau values for the contact resistance in the modeled system were of the order of tens of milli-Ohms, with initially rougher surfaces producing higher plateau contact resistances. While the calculated and experimental data were qualitatively similar, the quantitative behavior appeared to be very different. For example, scaling the experimental and calculated resistances to the same initial value did not produce overlaying curves. In a related paper, Brown *et al.* characterized the resistance of an Ohmic gold switch in an rf-MEMS device in the temperature range of 77–300 K.[3] At room temperature the device showed a similar drop in resistance with time as the switch used in Ref. 2.

In this paper we examine the computational and experimental resistances reported previously in Refs. 2 and 3 in terms of asperity creep. Our analysis shows that after a maximum of a few minutes, all of the experimental data near room temperature are well described by a power law in time and that the same power law relation with a similar exponent also describes the prior modeling data. This fitting suggests that while the apparent plateau regions define the practical contact resistances for most device applications, they do not, in fact, define the limiting resistances. Rather the plateaus are a consequence of the small exponential in the power law relations. Using an analytic single asperity model, it is shown that creep deformation can lead to the same power law relation and, more importantly, that the power law exponent can be directly calculated from the constitutive relation between creep rate and load. This analysis also shows that the prefactor in the power law relation depends on the initial surface structure.

a)Electronic mail: brenner@ncsu.edu.

II. ANALYSIS OF EXPERIMENTAL AND CALCULATED RESISTANCE DATA

Details of the computational plasticity model have been presented previously,[2] and therefore only a brief description is given here. A square contact with total dimensions of 4 μm^2 subject to a total load of 50 μN was assumed. These load and contact dimensions are based on the properties of the fabricated rf-MEMS switches described below. For simplicity, the two gold rough surfaces at the contact were replaced with a rough surface contacting a perfectly smooth surface. This is justified by the composite theory of roughness that demonstrates that with an appropriate transformation, a combined contact roughness can be replaced with a smooth plus rough interface.[4,5] Each asperity contact was treated independently, and the distribution of contact geometries was determined from a Weierstrass–Mandelbrot function.[6] The load on each individual asperity was determined by distributing the overall load according to the shapes and heights of the collection of asperities produced by a given set of roughness parameters. Two sets of roughness parameters were used that differed in the fractal roughness and dimension, as well as in the cutoff length that determined the maximum in the frequency index.

In the initial stages of the computation, the applied pressure was larger than the yield stress and therefore the asperities deformed plastically. For subsequent loading, the asperities deformed via creep with an assumed power law dependence of

$$\dot{\varepsilon} = C\sigma^p e^{(-Q_c/kT)}, \tag{1}$$

where $\dot{\varepsilon}$ is the creep rate, C depends on the material and creep mechanism, σ is the applied stress, p is the stress exponent, Q_c is the activation energy for creep, k is the Boltzmann constant, and T is the temperature. Redistribution of material at the contact due to creep was neglected for simplicity in the prior modeling. Therefore the resistances of individual asperities are slightly overestimated.

Because the dimensions of some the individual asperity contacts are of the order of the electron mean free path, an expression incorporating both the Maxwell and Sharvin resistance was used to calculate the resistance of an individual asperity.[7] This expression includes an interpolating function that depends on the ratio of the electron mean free path to the contact spot radius. A power law formulation was used to relate the resistivity of an asperity to strain hardening that included a temperature dependence to recovery and annihilation of stored dislocations due to plastic deformation. Two models were used to combine the resistances of the individual asperities. The first assumes that the contacts remain isolated and act in parallel. The second model replaces the collection of contacts with a single contact with area equal to the sum of the single asperity areas and a resistivity equal to the average of the individual contacts. The first and second models represent lower and upper limits to the true contact resistance, respectively.

Two different commercially available single pole double throw switches by wiSpry Inc. were used for the prior experimental measurements. Herein device 1 refers to the device used in Ref. 2, which is the original paper comparing the detailed modeling to the experimental device resistances; device 2 refers to the device used for the room temperature and low temperature experiments discussed in Ref. 3. To remove residual moisture, both devices were placed in a vacuum that was backfilled with helium and then held at a pressure of 760 Torr and a temperature of 293 K. A four point probe technique was used to measure resistance across the switches. Before the first measurement device 1 was cold switched (e.g., switched without an applied voltage) 250 times, and then a 100 μA dc current was applied across the device as the switch was held closed. The switch was then opened, cold switched 250 times, and closed again during a resistance measurement for two additional times for a total of three data measurements. For the data shown below, device two was cold switched 200 times, closed, and the resistance was measured with an applied 1 mA dc current. For both devices resistance measurements were taken each second from only one switch on the double throw for the duration of each experiment. Further manufacturing and operating details of these devices are given in the respective references.

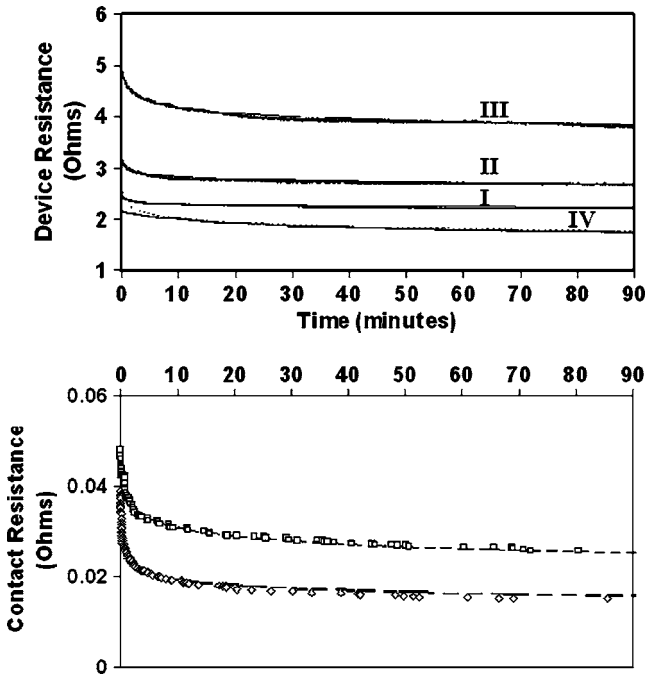

FIG. 1. Resistances across gold-gold contacts as a function of time. Bottom panel: Symbols denote calculated values from Ref. 2. The solid line is a fit of Eq. (2) to the computational data. Top panel: Solid lines are experimental measurements for a closed Ohmic switch in two rf-MEMS devices. Curves denoted I, II, and III correspond to the first, second, and third measurements on switch 1, respectively. The curve denoted by IV is for switch 2. Dashed lines represent fits of Eq. (2) to the experimental data. Except for the early stages of curve IV, the dashed and dotted lines are indistinguishable from one another on this graphing scale.

The results of the prior detailed computations were analyzed in terms of the time dependence of the ratio of the true to apparent contact areas, the number of contacting asperities, the size and shape of the asperities, the current through each asperity, and the total contact resistance. The latter was compared to the experimental measurements, and so the present analysis focuses on this relation. Plotted as the discrete points in the bottom panel of Fig. 1 is the calculated

TABLE I. Resulting parameters from the fit of Eq. (2) to the prior experimental and modeling data.

Fitting data	α	A (Ω min$^{\alpha}$)	B (Ω)
First measurement on switch 1 (curve I in top panel of Fig. 1)	0.073	0.45	1.90
Second measurement on switch 1 (curve II in top panel of Fig. 1)	0.073	1.08	1.90
Third measurement on switch 1 (curve III in top panel of Fig. 1)	0.073	2.68	1.90
Measurement on switch 2(curve IV in top panel of Fig. 1)	0.073	2.01	0.30
Computational data from Ref. 2. (bottom curve in bottom panel of Fig. 1)	0.094	0.024	0
Computational data from Ref. 2. (top curve in bottom panel of Fig. 1)	0.094	0.038	0

lower limit contact resistance for the two roughness models. Plotted as solids lines in the top panel is the measured resistances from the MEMS devices. Curves labeled I, II, and III denote measurements from the first, second, and third runs from device 1. The curve labeled IV is the measurement from device 2. As described above, each resistance curve shows an initial drop, followed by a plateau region. However, the resistances in each of the plateau regions are all different for the different roughness models and experimental runs. Furthermore, the experimentally measured device resistances are roughly two orders of magnitude larger than the calculated contact resistances.

Plotted as dotted lines in Fig. 1 are fits of the function

$$\rho = At^{-\alpha} + B \tag{2}$$

to all of the experimental measurements and the calculated resistances. The corresponding parameter values are given in Table I. Except for the first few minutes of curve IV, the fitted lines and the lines connecting the experimental measurements are indistinguishable from one another at this plotting scale. All four of the experimental fitting curves use the same value for α. For device 1, all three fitting curves use the same value for B with different A values. The fit to curve IV (device two) uses different A and B values. The fit of Eq. (2) to the calculated resistances is equally impressive. Both fitted expressions use the same values for α and B, and different A values.

The relatively accurate fit provided by Eq. (2) to both the detailed modeling and experimental measurements suggests that the resistance as a function of time of the gold Ohmic contact within these devices can be understood from a few properties of the switch. Parameter B represents the resistance in the $t=\infty$ limit. For the computational results, which directly yield the contact resistance, a value of zero for B implies that the limiting resistance corresponds to an ideal interface at which the asperities have been completely flattened and plastic damage removed. The experimental studies, on the other hand, measure the total resistance of the device, hence yielding a combination of the contact resistance across the switch and other resistance contributions from the device. The common value of B for all three runs for device 1 supports this interpretation. Adding the resistances of the wire bond and the conduction path within the device (excluding the contact resistance across the switch) yields an estimate for the device resistance of 1.54 Ω, which is intermediate between the fitted B values for the two devices (both of which are from the same wySpry design).

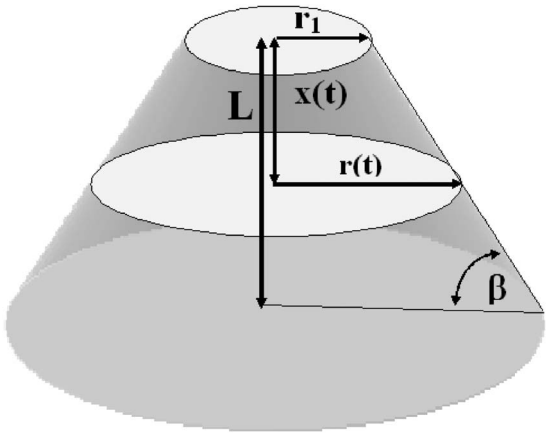

FIG. 2. Illustration of the conical geometry used in the single asperity model. L and r_1 are the initial asperity height and radius, respectively, β is the angle of the side of the asperity with respect to the surface plane, and $x(t)/L$ and $r(t)$ are the time-dependent strain and radius, respectively.

The common value of α for the experimental curves, and the small difference between the experimental and computational values, suggests that this parameter reflects an intrinsic material property of the gold in the switch. The two roughness models used in the computational studies yield different values for A in Eq. (1), suggesting that this parameter reflects the initial state of the surfaces prior to contact. Interestingly, the rougher surface yields a higher A value. This is discussed more below.

III. ANALYTIC SINGLE ASPERITY MODEL

The following analytic single asperity deformation model can be used to derive the form of Eq. (2). More importantly it demonstrates the origin of the α and A parameters. The geometry of the model is illustrated in Fig. 2. It is composed of a single conical asperity with initial height L and radius r_1 whose shape is designated by the angle β with respect to the interface plane. This assumed geometry is used because it leads to a relatively straightforward derivation that justifies Eq. (2). The time-dependent strain is defined as the change in height $x(t)$ normalized by the initial asperity height L. With this definition the strain rate is given by

$$\dot{\varepsilon}(t) = \frac{\dot{x}(t)}{L}, \tag{3}$$

and the stress due to load F on the asperity is defined as

$$\sigma = \frac{F}{\pi r^2(t)}. \tag{4}$$

With this geometry

$$\dot{r}(t) = \frac{\dot{x}(t)}{\tan(\beta)}, \tag{5}$$

which combined with Eq. (3) leads to

$$\dot{\varepsilon}(t) = \frac{\tan(\beta)}{L}\dot{r}(t). \tag{6}$$

Substituting Eqs. (4) and (6) into Eq. (1) gives

$$\dot{r}(t) = Ce^{(-Q_c/kT)}\left(\frac{L}{\tan(\beta)}\right)\left(\frac{F}{\pi r^2(t)}\right)^p, \tag{7}$$

which can be integrated with respect to time to yield the relation

$$r(t) = \left[\left(\frac{LCe^{(-Q_c/kT)}F^p(1+2p)}{\tan(\beta)\pi^p}\right)t + r_1^{(1+2p)}\right]^{1/(1+2p)}, \tag{8}$$

for the radius as a function of time. Equation (8) reduces to the initial asperity radius for time $t=0$ and is only valid for $r(t)$ less than or equal to the radius of the base of the asperity (i.e., strains between 0 and 1). If r_1 is sufficiently small, $r_1^{(1+2p)}$ can be ignored with respect to the first term in the brackets in Eq. (8) at some finite time, which yields

$$r(t) = \left(\frac{LCe^{(-Q_c/kT)}F^p(1+2p)}{\tan(\beta)\pi^p}\right)^{1/(1+2p)} t^{1/(1+2p)}, \tag{9}$$

for Eq. (8). Finally, combining Eq. (9) with a Maxwell spreading resistance $R(t)$ of the form[8]

$$R(t) = \frac{\rho}{2r(t)} \tag{10}$$

gives a time-dependent resistance due to creep of the form

$$R(t) = \frac{\rho}{2\left(\frac{LCe^{(-Q_c/kt)}F^p(1+2p)}{\pi^p\tan(\beta)}\right)^{1/(1+2p)}} t^{-1/(1+2p)}. \tag{11}$$

Equating Eq. (11) to Eq. (2) yields

$$A = \frac{\rho}{2}\left(\frac{LCe^{(-Q_c/kt)}F^p(1+2p)}{\pi^p\tan(\beta)}\right)^{-1/(1+2p)} \tag{12}$$

and

$$\alpha = \frac{1}{1+2p}. \tag{13}$$

By using Eq. (10) the contribution of the Sharvin resistance is neglected compared to the Maxwell spreading resistance. The overall contact resistance is governed by the asperity with the lowest resistance and hence largest contact area, which is where the Sharvin resistance is smallest compared to the Maxwell spreading.

The form of Eqs. (12) and (13) supports observations made above regarding the physical origin of the A and α parameters in Eq. (2), and it provides a plausible explanation for why the A value increased for multiple measurements on switch 1. It was suggested above that α in Equation (2) is related to an intrinsic property of the material out of which the switch is composed. Equation (13) suggests that this is indeed the case and that the value for α can be specifically related to the creep coefficient in Eq. (1). The values of α of 0.073 determined by fitting to the experimental data and 0.094 by fitting the plasticity model give creep coefficients of 6.35 and 4.82, respectively. Creep coefficients are typically between about 4 and 10 depending on the creep mode. Also from Eq. (13) the value of A in Eq. (2) is proportional to $[L/\tan(\beta)]^{-\alpha}$. Therefore larger angles of the asperities with respect to the surface plane, which correspond to rougher surfaces, produce larger A values, consistent with the detailed plasticity modeling.[2] Finally Eq. (13) implies that for the same angle, shorter asperities produce larger A values in Eq. (2). This result suggests that asperity blunting contributes to the increasing A values observed for device 1 for the second and third runs. However, this does not explain why for each consecutive run the initial resistance increases. This could be due to roughening during switch opening, the formation of a contamination film after opening,[7,9] or some other contribution (or combination of contributions).

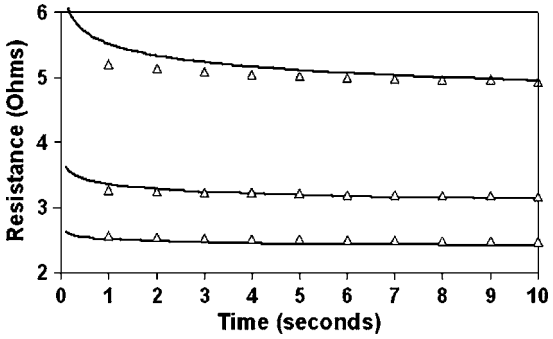

FIG. 3. Curves I–III from Fig. 1 for the first 10 s. Symbols are the experimental data; solid lines are the fit of Eq. (2) to each entire data set.

The approximation that leads from Eq. (8) to Eq. (9) for this single asperity model yields a prediction for the contact resistance that has not been previously recognized. For multiple switching, the blunting of asperities decreases the value of the first term and increases the value of the second term in the brackets in Eq. (8). Hence this analysis predicts that it will take a longer time [i.e., a larger value for t in the first term in the brackets in Eq. (8)] for the contact resistance to attain a power law relation with each successive closing of the switch. Plotted in Fig. 3 is a blow-up of the experimental data plotted in Fig. 1 for device 1 (curves I–III) during the first 10 s of switch operation. The solid lines are the results of Eq. (2) with parameters fit to the entire 90 min data run as described above. For curve I, which is the first closing of the switch, the power law relation for the entire run fits the first few data points very well. For the second closing (middle plot), the experimental measurement is flatter than the power law prediction up until about 4 s, after which the power law provides a good description of the data. The same trend is seen for the third switching (the top plot), except that it requires about 9 s for the experimental data to be well described by the power law. This behavior qualitatively matches the prediction of our single asperity analytic analysis.

IV. SUMMARY

We have shown that the measured resistance as a function of time for two MEMS switches as well as a comparable resistance calculated using a specialized finite-element plasticity model is well described by a power law relation. This

relation is derived analytically from a single asperity model, which demonstrates that the coefficient of the power law is directly related to the creep coefficient and that the prefactor to the power law is related to the initial roughness of the contact. The analytic model also predicts a transition from a constant contact resistance to the power law that occurs at increasingly longer times for successive switch opening and closing that is caused by asperity blunting. Analysis of the first few seconds of the measured resistance for three successive openings and closings of one of the MEMS devices supports this prediction. This work thus provides guidance toward the rational design of Ohmic contacts with enhanced reliabilities by better defining variables that can be controlled through material selection, interface processing, and switch operation.

ACKNOWLEDGMENTS

Interactions with Art Morris of WiSpry Inc. are gratefully acknowledged. This work has been supported by the Extreme Friction MURI program, AFOSR Grant No. FA9550-04-1-0381 entitled "Multifunctional Extreme Environment Surfaces: Nanotribology for Air and Space. C.B. and J.K. were also supported by the DARPA Center for rf MEMS reliability and Design Fundamentals Grant No. HR0011-06-1-0051.

[1]See, for example, G. M. Rebeiz, *RF MEMS: Theory, Design and Technology* (Wiley, Hoboken, 2003).
[2]O. Rezvanian, M. Zikry, C. Brown, and J. Krim, J. Micromech. Microeng. **17**, 2006 (2007).
[3]C. Brown, A. S. Morris, A. I. Kingon, and J. Krim, "Cryogenic Performance of RF MEMS Switch Contacts," J. Microelectromech. Syst. (in press).
[4]H. A. Francis, Wear **45**, 221 (1977).
[5]M. O'Callaghan and M. A. Cameron, Wear **36**, 79 (1976).
[6]W. Yan and K. Komvopoulos, J. Appl. Phys. **84**, 3617 (1998).
[7]B. D. Jenson, L. L.-W. Chow, K. Huang, K. Saitou, J. L. Volarkis, and K. Kurabayashi, J. Microelectromech. Syst. **14**, 935 (2005).
[8]*Electrical Contacts: Principles and Applications* edited by P. G. Slade (Dekker, New York, 1999).
[9]H. P. Koidl, W. F. Rieder, and Q. R. Saltzmann, IEEE Trans. Compon. Packag. Technol. **22**, 439 (1999).